PERGAMON

International Journal of Heat and Mass Transfer 42 (1999) 3019–3035

International Journal of HEAT and MASS TRANSFER

Experimental study on interfacial area transport in bubbly two-phase flows

Takashi Hibiki[a], Mamoru Ishii[b,*]

[a]*Research Reactor Institute, Kyoto University, Kumatori, Sennan, Osaka, 590-0494, Japan*
[b]*School of Nuclear Engineering, Purdue University, West Lafayette, IN 47907-1290, USA*

Received 15 May 1998; received in revised form 21 December 1998

Abstract

In relation to the development of the interfacial area transport equation, local measurements of the void fraction, interfacial area concentration, interfacial velocity, and Sauter mean diameter using the double sensor probe method as well as the liquid velocity and turbulence intensity using hotfilm anemometry, were performed extensively for vertical upward bubbly air–water flows in a round tube with an inner diameter of 25.4 mm at three axial locations of $L/D=12.0$, 65.0 and 125, and fifteen radial locations from $r/R=0$ to 0.95. The liquid flow rate and the void fraction ranged from 0.292 m/s to 3.49 m/s and from 3% to 27%, respectively. The data set obtained in this study will eventually be used for the development of reliable constitutive relations which reflect the true transfer mechanisms in bubbly flow systems.

Keywords: Interfacial area transport; Two-fluid model; Void fraction; Interfacial area concentration; Bubble size; Turbulence; Local measurement; Resistivity probe; Hotfilm anemometry; Gas–liquid flow; Pipe flow; Bubbly flow; Multiphase flow

1. Introduction

Two-phase flow is characterized by the existence of an interface between phases and discontinuities of properties associated with them. The internal structures of two-phase flows are identified by two-phase flow regimes. Various transfer mechanisms between the mixture and wall as well as between phases strongly depend on these two-phase flow regimes. This leads to the use of flow regime dependent correlations and closure equations together with appropriate flow regime transition criteria. The basic structure of flow can be characterized by two fundamental geometrical parameters. These are the void fraction and interfacial area concentration. The void fraction expresses the phase distribution whereas the interfacial area describes the available area for the interfacial transfer of mass, momentum and energy. Therefore, an accurate knowledge of these parameters is necessary for any two-phase flow analysis. This fact can be further substantiated with respect to two-phase flow formulation.

The two-fluid model is formulated by considering each phase separately in terms of two sets of conservation equations which govern the balance of mass, momentum and energy of each phase. These balance equations represent the macroscopic fields of each phase and are obtained from proper averaging

* Corresponding author. Tel.: +1-765-494-4587; fax: +1-765-494-9570.

E-mail addresses: hibiki@rri.kyoto-u.ac.jp (T. Hibiki), ishii@ecn.purdue.edu (M. Ishii)

0017-9310/99/$ - see front matter
PII: S0017-9310(99)00014-9

Nomenclature

a_i	interfacial area concentration
D	pipe diameter
D_B	bubble diameter
D_{Sm}	Sauter mean diameter
Eo	Eötvös number
F	sampling frequency
$I(\omega_0)$	correction factor
j_g	superficial gas velocity
j_f	superficial liquid velocity
L	length along flow direction
N_t	number of bubbles which pass the point per unit time
n	bubble number density
P	pressure
R	pipe radius
R_B	bubble radius
r	radial coordinate
S_j	source or sink terms in the interfacial area concentration due to bubble breakup or coalescence, respectively
S_{ph}	source or sink term in the interfacial area concentration due to phase change
v_g	interfacial velocity
$\vec{v}_g$	average local bubble velocity weighted by the bubble number
v_{iz}	z component of interfacial velocity
v_f	liquid velocity
v_f'	liquid turbulent fluctuation
v_{sz}	passing velocity of jth interface through the double sensor probe in mean flow direction
z	z coordinate

Greek symbols

α	void fraction
β	volumetric flow rate quality
δ_B	distinguishable liquid-layer thickness between bubbles by double sensor probe
η	correction factor
ξ	interfacial area change due to bubble coalescence or breakup
σ_z	root mean square of fluctuations of z component interfacial velocity
τ	minimum response time of the circuit
ψ	factor depending on the shape of a bubble ($1/36\pi$ for a spherical bubble)
ω_0	maximum angle between velocity vector of jth interface and mean flow direction vector

Subscripts

0	inlet
B	small bubble
C	cap bubble
eq	equilibrium state
max	maximum value

Mathematical symbols

$\langle\ \rangle$	area average
-t	time average

methods. Since the macroscopic fields of each phase are not independent of the other phase, the phase interaction terms which couple the transport of mass, momentum and energy of each phase appear in the

field equations. It is expected that the two-fluid model can predict mechanical and thermal nonequilibrium between phases accurately. However, it is noted that the interfacial transfer terms should be modeled accurately for the two-fluid model to be useful. In the present state of the arts, the closure relations for these interfacial terms are the weakest link in the two-fluid model. The difficulties arise due to the complicated transfer mechanisms at the interfaces coupled with the motion and geometry of the interfaces. Furthermore, the closure relations should be modeled by macroscopic variables based on proper averaging.

In general, the interfacial transfer terms are given in terms of the interfacial area concentration a_i and driving force [1]:

$$\text{(Interfacial transfer term)} \sim a_i \times \text{(driving force)}$$

The area concentration defined as the interfacial area per unit volume of the mixture characterizes the first order geometrical effects; therefore, it must be related to the internal flow-pattern of the two-phase flow field. On the other hand, the driving forces for the interfacial transport characterize the local transport mechanisms such as the turbulence, molecular transport properties and driving potentials. In two-phase flow systems, the void fraction and interfacial area concentration are two of the most important geometrical parameters. The interfacial area concentration should be specified by a closure relation, or by a transport equation. The above formulation indicates that the knowledge of the interfacial area concentration and the interfacial structure classified as the flow regimes are indispensable in the two-fluid model. Various transfer mechanisms between phases depend on the two-phase flow interfacial structures. The geometrical effects of interfacial structure can be modeled in a macroscopic field by the interfacial area concentration and void fraction. In order to take into account the effect of entrance, developing flow, coalescence and disintegration, and wall nucleation source, an introduction of the interfacial area transport equation is recommended [2].

In view of its great importance to two-fluid model, the interfacial area concentration has been studied intensively over the past ten years. The development of the source and sink terms in the transport equation heavily depends on understanding the mechanisms of bubble coalescence and disintegration as well as obtaining accurate experimental data for the changes in the interfacial area. As to the theoretical study, Kocamustafaogullari and Ishii derived the interfacial area transport equation from the statistical model of fluid particle number transport equation [2]. The resulting equation includes the source and sink terms due to the particle interactions and interfacial phase change. Ishii et al. proposed a preliminary model on the source and sink terms of the one-dimensional interfacial area transport in an adiabatic bubbly flow and compared their model with an experimental data [3–5]. As to the experimental study, accurate data sets of local flow parameters such as void fraction, interfacial area concentration, interfacial velocity, bubble diameter, liquid velocity and turbulence intensity are indispensable to develop the source and sink terms of the interfacial area transport equation. Although much two-phase data has been taken for local void fraction, local interfacial area, and average bubble size, there have been few if any attempts to relate these local parameters to local transport mechanisms like turbulent diffusion [6–12]. The main reason for this lack of data has been the inability to effectively measure the liquid turbulence in the presence of dispersed gas bubbles. In addition to this, only a limited number of data set is available for axial development of flow parameters so far [13–15]. A detailed literature review of local flow measurements in two-phase bubbly flow systems is given in the previous report [16].

From this point of view, measurements of vertical upward air–water bubbly flows in a round tube with an inner diameter of 25.4 mm were performed by using the double sensor and hot film probes. The combined data from the double-sensor probe and the hot film probe give near complete information on the time averaged local hydrodynamic parameters of two-phase flow. This data will be used for the development of reliable constitutive relations which reflect the true transfer mechanisms in the two-phase flow.

2. Experimental

2.1. Double sensor probe methodology

Local flow parameters such as void fraction, bubble diameter, interfacial velocity and interfacial area concentration were measured by a double sensor probe. The double sensor probe was basically used as a phase identifier of the two-phase mixture. The double sensor probe consisted of two sensors made of platinum–rhodium (13% Rh) wire with a diameter of 0.127 mm. The two wires were adjusted for a typical distance of approximately 2–3 mm in the length wise direction and were aligned in the axial direction. The information to be recorded from each signal was the number of bubbles that had hit the sensor, the time that the sensor was exposed to the gas phase, and the relative time between the bubble hitting the upstream and downstream sensor. The time-averaged interfacial velocity v_g was calculated by taking into account the distance between the tips of the upstream and downstream sensor and the time difference between the upstream and downstream signal. The time-averaged

void fraction α was simply the accumulated time the sensor was exposed to the gas phase divided by the total sampling time of the sensor. It has been shown mathematically that the interfacial area concentration a_i equals the harmonic mean of the interfacial velocity. The theoretical base of this measurement technique was given by Kataoka and Ishii [17]. Recently, the basic equation has been improved by Wu and Ishii [18], and Hibiki and Ishii [14]. The following equation can be derived based on the assumption that the number of measured interfaces is large, interfacial velocity is statistically independent of the angle between mean flow direction (z direction) and normal direction of jth interface, the interfaces are composed of spherical bubbles, the probe passes every part of a bubble with an equal probability and transverse direction (x or y direction) components of interfacial velocity are random [14].

$$a_i = 2N_t \overline{\frac{1}{|\vec{v}_{sz}|}}^t I(\omega_0), \quad I(\omega_0) = \frac{\omega_0^3}{3(\omega_0^3 - \sin\ \omega_0)} \tag{1}$$

where N_t, v_{sz}, and ω_0 denote the number of bubbles which pass the point per unit time, the passing velocity of the jth interface through the double sensor probe in the z direction, and the maximum angle between the velocity vector of the jth interface and z direction vector, respectively. The relationship between the maximum angle and the interfacial velocity can be derived based on the assumption that the root mean square of the fluctuations of the z component interfacial velocity σ_z is equal to that of the root mean square of the x and y component velocity fluctuations.

$$\frac{3}{2\omega_0^2}\left(1 - \frac{\sin\ 2\omega_0}{2\omega_0}\right) = \frac{1 - (\sigma_z^2/\overline{|\vec{v}_{iz}|}^{t^2})}{1 + 3(\sigma_z^2/\overline{|\vec{v}_{iz}|}^{t^2})} \tag{2}$$

The interfacial area concentration can be calculated from the number of bubbles which pass the point per unit time, and the interfacial velocity with Eqs. (1) and (2). The Sauter mean diameter D_{Sm} can be expressed as a function of the time-averaged interfacial area concentration and void fraction, namely $D_{Sm} = 6\alpha/a_i$.

In the strict sense, the assumption of spherical bubbles may not be valid for any bubbly flow systems. Bubble shapes in the present experiment may be ellipsoidal with wobbling interfaces. However, it is considered that the assumption would practically work for the interfacial area concentration measurement on the following grounds. The area averaged interfacial area concentrations measured by the double sensor probe method were compared with those measured by a photographic method in relatively low void fraction ($\langle\alpha\rangle \leqslant 8\%$) and wide liquid velocity ($0.262\ \text{m/s} \leqslant j_f \leqslant 3.49\ \text{m/s}$) conditions where the photographic method could be applied [14]. Good agreement was obtained between them within the relative deviation of 6.95%. In addition to this, when a spherical bubble is transformed into an ellipsoidal bubble with the aspect ratio of 2, the resulting increase of the interfacial area is estimated mathematically to be less than 10% [19].

As for the assumption of isotropic turbulence, the study carried out by Hilgert and Hofmann [20] for bubbly flow in a vertical pipe using the ultrasonic Doppler technique, has shown that the magnitude of the axial component of the root mean squares of bubble velocity fluctuation is nearly equal to the transverse components of the root mean squares of the fluctuations of bubble velocity at low superficial gas velocities. Several researches on the interfacial area measurement have been performed by the double sensor probe method based on the assumption of spherical bubbles [13–17,21–24]. However, it is considered that future studies should focus on rigorous formulation of the interfacial area concentration taking account of the bubble shape with deformed interface, and measurement of local liquid turbulence over wide range of flow conditions.

Using a fast A/D converter Metrabyte DAS-20 board and an IBM/PC-XT computer, local flow measurements were conducted in a data acquisition program. The acquisition board has a maximum sampling rate of 100,000 cycles per second. For the data sets measured with the double sensor probe, a minimum of 2000 bubbles were sampled to maintain similar statistics between the different combinations of gas flow rates. Here, in the void fraction measurement at bubbly-to-slug flow transition, bubbles were separated into either a Taylor bubble or a small bubble based on the double-sensor probe signals [24]. The determination as to whether detected bubbles were cap bubbles was performed based upon the chord length of bubbles. According to Clift's shape regime map for bubbles [25], the boundary between ellipsoidal and spherical-cap bubbles is given by $Eo = 40$, which corresponds to the bubble diameter of 17.2 mm at 20°C. In the present experiment, when local bubble chord length exceeded 15 mm, bubbles were considered as cap bubbles. Thus, the void fraction for each category was obtained separately. It should be noted here that the signals for cap bubbles were not acquired in the measurement of the interfacial area concentration as well as the Sauter mean diameter but the void fraction. The contribution of cap bubbles to total interfacial area concentration would be relatively small (see Appendix). Therefore, it is expected that even data taken at the bubbly-to-slug transition would be used for evaluation of modeled sink and source terms in one-group interfacial area transport equation.

In the measurement using the double sensor probe, the distinguishable liquid-layer thickness between

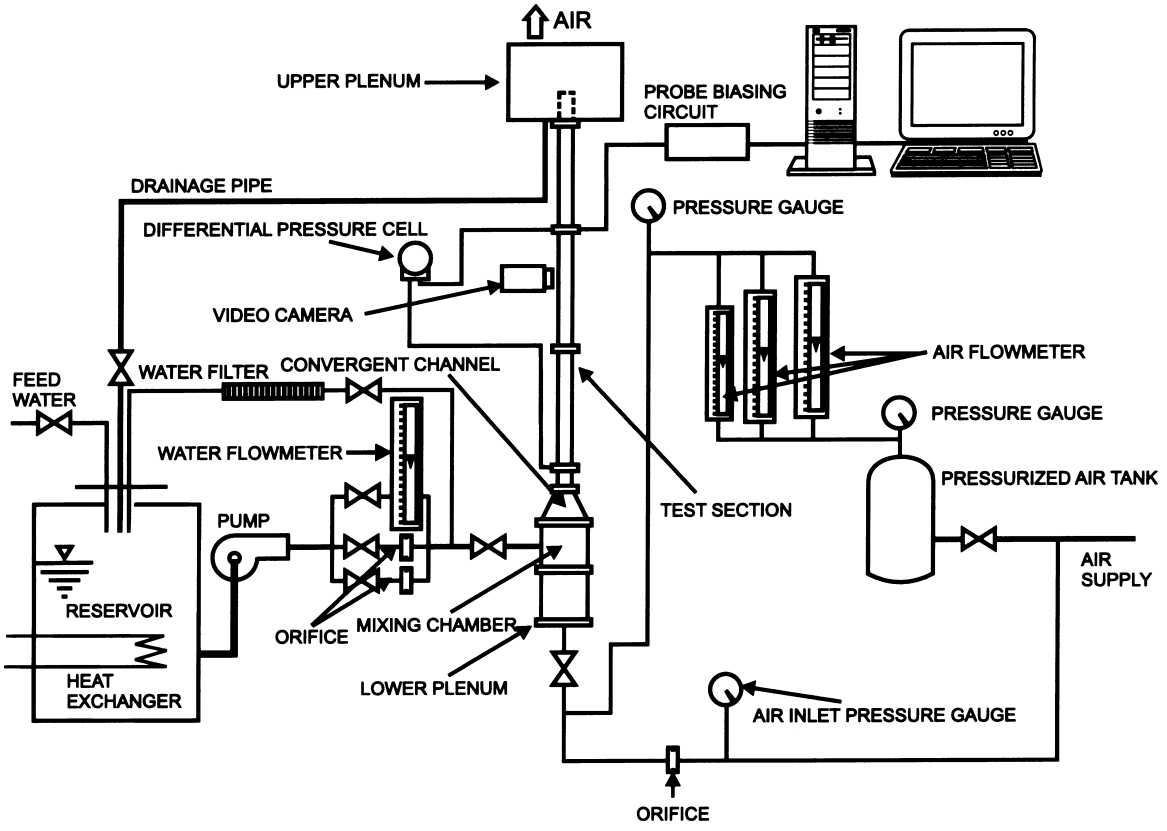

Fig. 1. Schematic diagram of experimental loop.

bubbles δ_B may be roughly estimated by the interfacial velocity v_g, the sampling frequency f and the minimum response time of the circuit τ, that is $\delta_B \approx \max[v_g/f, v_g\tau]$. In the present data acquisition system, the distinguishable liquid-layer thickness between bubbles is roughly estimated to be 0.3 mm. Therefore, the double sensor probe may not distinguish each bubble in a large bubble cluster consisted of a cap bubble and small bubbles at the bubbly-to-slug flow transition boundary, when they are tightly packed. The double sensor probe methodology was detailed in the previous paper [14,19,21].

It should be noted here that the double sensor probe method may not work in the vicinity of a wall. The presence of the wall does not allow a bubble to pass the probe randomly as in the other positions in the pipe. This fact will cause a measurement error in the interfacial area concentration, interfacial velocity and Sauter mean diameter. The range where the double sensor probe method can work may be roughly estimated as $0 \leqslant r/R \leqslant 1-R_B/R$, where R_B denotes the bubble radius. In this experiment ($D=25.4$ mm), the effective range of the double sensor probe is $0 \leqslant r/R \leqslant 0.84$ or $0 \leqslant r/R \leqslant 0.92$ for $R_B=2$ mm or 1 mm , respectively. The detailed discussion was given by Kalkach-Navarro et al. [22].

2.2. Hotfilm anemometer methodology

Local flow parameters such as liquid velocity v_f and liquid velocity fluctuation v_f' in a two-phase flow were measured by using a hotfilm anemometer system FlowPoint, which TSI Incorporated developed for liquid velocity and turbulence intensity measurements in a single-phase flow. The FlowPoint system is a fully-integrated, thermal anemometer-based system that measures the local fluid velocity and local fluid temperature. The probes used in this experiment were the TSI Model 1264 AW designed with a conical tip. The tip had a sensor diameter of 1.27 mm and a sensor length of 1 mm. The hotfilm probe was calibrated with an electromagnetic flow meter. In order to obtain the liquid velocity representative of the flow, it was necessary to filter out the voltage depressions and spikes due to the bubbles hitting and passing the probe. The voltage spikes were removed from the signal using threshold and maximum slope schemes. After the bubbles were removed from the signal, the voltages

Table 1
Flow conditions in this experiment[a]

Symbols	●	▲	■	▼	◆
j_f [m/s]	$j_{g,0}$ [m/s]	$j_{g,0}$ [m/s]	$j_{g,0}$ [m/s]	$j_{g,0}$ [m/s]	$j_{g,0}$ [m/s]
0.262	0.0549 (13.7)	0.0610 (15.4)	0.0780 (19.2)	0.0990 (23.2)	0.117 (26.6)
0.872	0.0414 (5.09)	0.0813 (9.35)	0.143 (15.2)	0.210 (20.6)	0.305 (26.8)
1.75	0.0461 (3.14)	0.116 (7.31)	0.257 (14.4)	0.399 (19.7)	0.575 (25.2)
2.62	0.0804 (3.56)	0.193 (7.87)	0.401 (14.6)	0.581 (19.7)	0.764 (24.2)
3.49	0.0509 (1.83)	0.201 (6.57)	0.516 (15.1)	0.702 (19.5)	0.931 (24.2)

[a] Values in the parentheses indicate the void fractions in % measured at $L/D = 125$.

from the hotfilm probe were converted to velocities using the calibration curve and the statistical parameters identifying the turbulent flow was calculated. In this study, the turbulence intensity was identified by $v_f'/v_{f,max}$. The hotfilm anemometer methodology was detailed in the previous paper [14, 26].

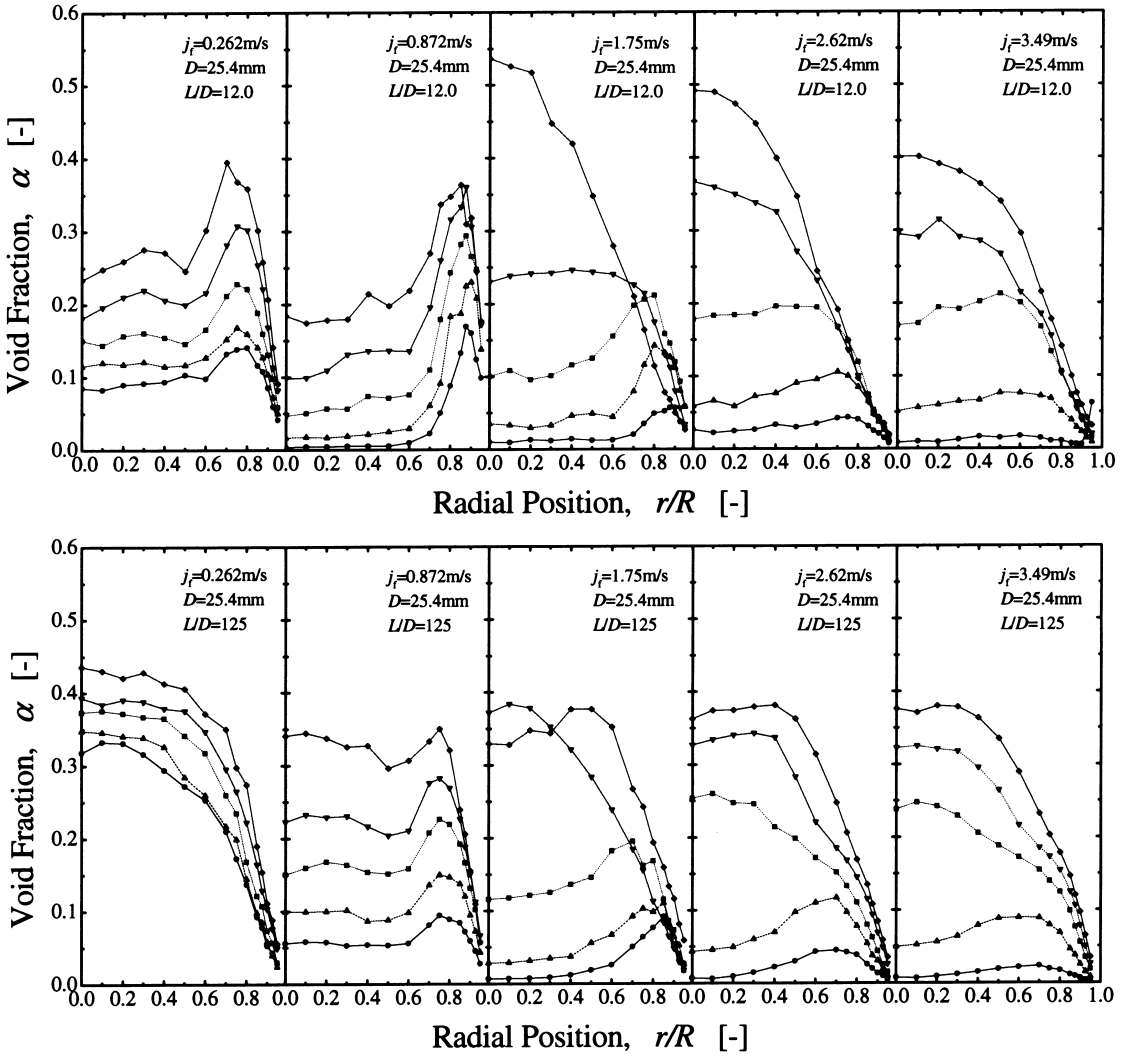

Fig. 2. Local void fraction profiles at $L/D = 12.0$ and 125.

2.3. Two-phase flow experiment

Fig. 1 shows the schematic diagram of a two-phase flow loop. The test section was a round tube made of an acrylic resin. Its inner diameter and length were 25.4 and 3750 mm, respectively. Air was supplied by a compressor and was introduced into a mixing chamber through a porous media with the pore size of 40 μm. The air and purified water were mixed in the mixing chamber and the mixture flowed upwards through the test section. After flowing through the test section, the air was released into the atmosphere through a separator, while the water was circulated by a centrifugal pump. The flow rates of the air and water were measured with a rotameter and a magnetic flow meter, respectively. The loop temperature was kept at a constant temperature (20°C) within the deviation of ±0.2°C by a heat exchanger installed in a water reservoir. The local flow measurements using the double sensor and hotfilm probes were performed at three axial locations of $L/D=12.0$, 65.0, and 125 and fifteen radial locations from $r/R=0$ to 0.95. The pressure measurements were also conducted by Bourdon-tube pressure gauges at the above three measuring stations. The superficial liquid velocities j_f and the inlet superficial gas velocities $j_{g,0}$ in this experiment are tabulated in Table 1. The flow conditions covered most of a bubbly flow region, including bubbly-to-slug transition region. The superficial gas velocities were roughly determined so as to provide the same void fractions among different conditions of superficial liquid velocity, namely $\alpha_{L/D=125}=3$, 7, 15, 20, and 25%. For $j_f=0.262$ m/s, void fraction could not be set at less than 10% because of a very low gas flow rate, which could not be regulated by the present loop. It should be noted here that the void fraction increased along the axial direction on the order of 20–40% between $L/D=12.0$ and 125 in the present experimental conditions due to the pressure reduction. This led to a continuous developing flow along the flow direction.

In order to verify the accuracy of local measurements, the area averaged quantities obtained by integrating the local flow parameters over the flow channel were compared with those measured by the other cross-calibration methods [14]. Good agreements were obtained between the area averaged void fraction, interfacial area concentration and Sauter mean diameter, velocity, and liquid velocity obtained from the local measurements and those measured by the γ-densitometer, the photographic method, the rotameter and the magnetic flow meter within the error of 5.74, 6.95, 12.4, and 5.19%, respectively.

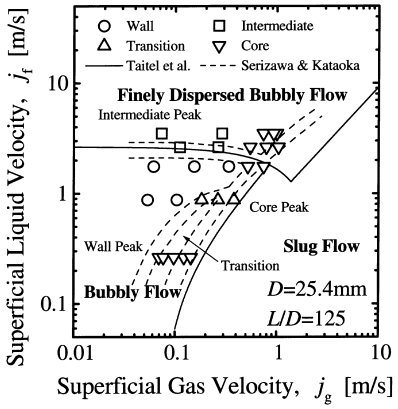

Fig. 3. A map of phase distribution patterns.

3. Results and discussion

3.1. Local flow parameters

3.1.1. Void fraction

An initial condition (bubble size, generation method and mixing condition), a flow condition (flow rates and physical properties), and a test section condition (geometry and wall surface) generally affect a void distribution [27,28]. Fig. 2 shows the behavior of void fraction profiles measured at $L/D=12.0$ (upper figures) and 125 (lower figures) in this experiment. Serizawa and Kataoka roughly classified the phase distribution pattern into four basic types of distributions [29]. Fig. 3 shows a map of phase distribution patterns determined based on the definition by Serizawa and Kataoka. The symbols of circle, triangle, square, and reversed triangle in Fig. 3 indicate the wall peak, the intermediate peak, the core peak, and the transition, respectively, observed at $L/D=125$ in this experiment. The solid and broken lines in Fig. 3 mean the flow regime transition boundaries predicted by the model of Taitel et al. [30] and phase distribution pattern transition boundaries given by Serizawa and Kataoka [29], which were determined based on experiments performed by different researchers with different types of bubble injections in round tubes ($20\ \text{mm} \leqslant D \leqslant 86.4\ \text{mm}$). A fairly good agreement was obtained between the Serizawa–Kataoka's map [29] and observed phase distribution patterns.

Fig. 4 shows the behavior of Sauter mean diameter profiles, corresponding to that of void fraction profiles in Fig. 2. A cap bubble was formed in the high void fraction region as shown in Fig. 5. In this experiment, the formation of cap bubbles started at $\langle\alpha\rangle \approx 15\%$. It should be noted here that the Sauter mean diameter in the high void fraction region was calculated from void fraction and interfacial area concentration for bubbles

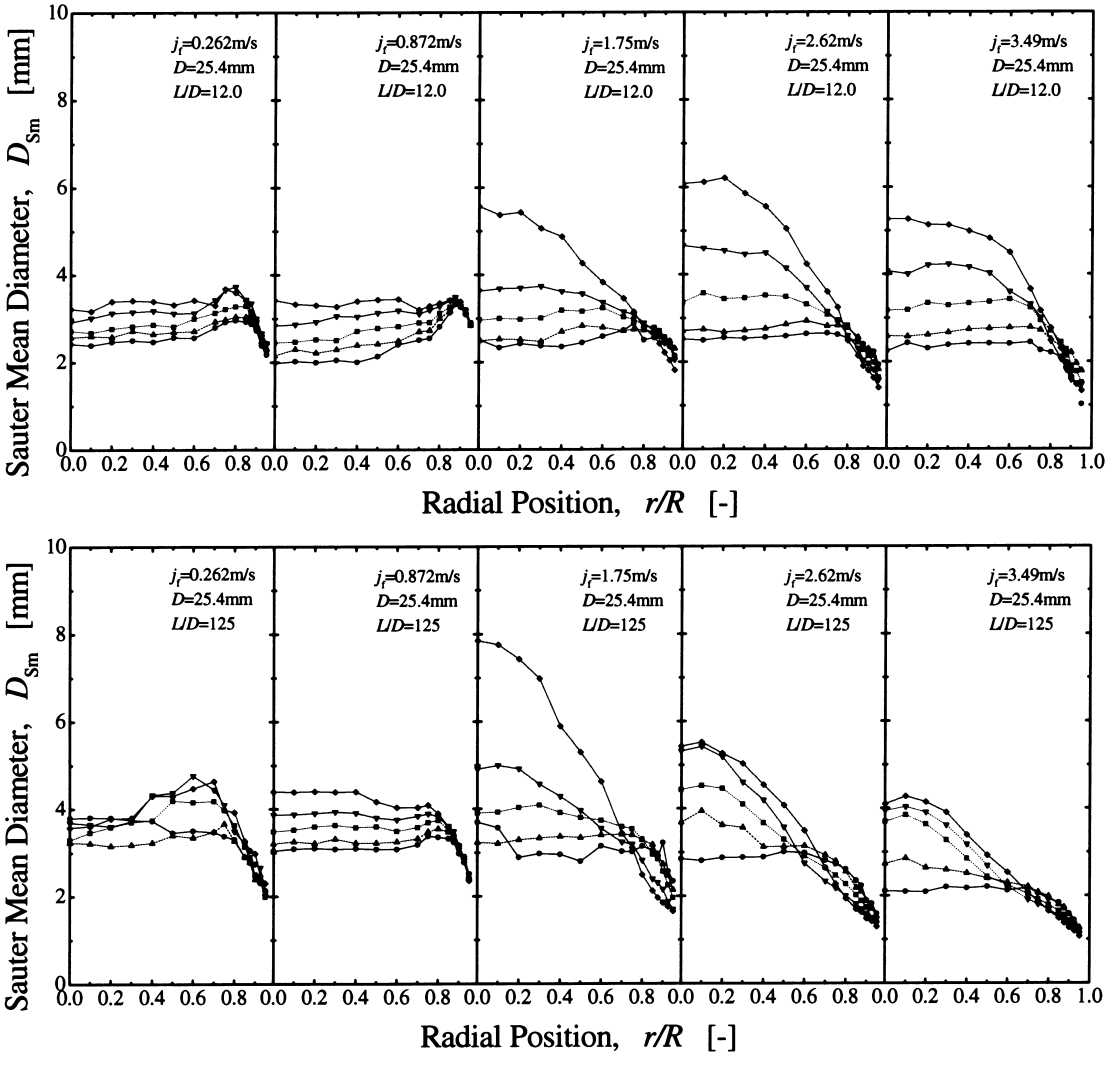

Fig. 4. Local Sauter mean diameter profiles at $L/D = 12.0$ and 125.

except for cap bubbles, that is $D_{Sm} = 6(\alpha - \alpha_C)/(a_i - a_{i,C})$ as mentioned in Section 2.1. Fig. 6 shows the axial development of one-dimensional Sauter mean diameters $\langle D_{Sm} \rangle$ (upper figure) obtained by integrating local Sauter mean diameter over the flow channel.

For $j_f = 0.262$ m/s (● ▲, ■, ▼, ◆), 0.872 m/s (●, ▲, ■, ▼, ◆), and $j_f = 1.75$ m/s and $\alpha < 20\%$ (●, ▲, ■), the wall peak in the void fraction profile was observed at the first measuring station, $L/D = 12.0$ (see Fig. 2). In the flow condition, local Sauter mean diameter for the flow condition was smaller than about 3.5 mm as shown in Fig. 4. For such low liquid velocities, liquid turbulence would mainly contribute to promotion of collision between bubbles, resulting in enhanced bubble coalescence, since it might not have enough energy to break up bubbles. Thus, the bubble diameter was gradually increased along the flow direction due to bubble coalescence and expansion as shown in Fig. 6. Since a large bubble tends to migrate toward the tube center, the increase in bubble size along the flow direction changes the void distribution [29,31]. When the area averaged void fraction was smaller than 10% ($j_f = 0.872$ m/s, ●, ▲; $j_f = 1.75$ m/s, ●, ▲), the bubble coalescence might not be marked because of large distances between bubbles. In this case, local Sauter mean diameter did not exceed 3.5 mm, resulting in the wall peak at $L/D = 125$. The peaks were approximately located at a distance equal to the bubble radius (for example, the peak location for 4 mm diameter bubble is $r/R = 0.85$). The void peak tended to move toward the pipe center and diminished as the bubble size increased along the flow

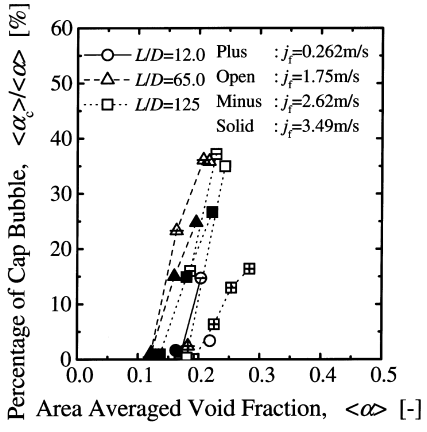

Fig. 5. Percentage of void fraction in a form of cap bubble $\langle\alpha_C\rangle$.

direction. On the other hand, for void fraction higher than 10% ($j_f = 0.262$ m/s, ●, ▲, ■, ▼, ◆; $j_f = 0.872$ m/s, ■, ▼, ◆; $j_f = 1.75$ m/s, ■), local Sauter mean diameters exceeded 3.5 mm at $L/D = 125$ (see Fig. 4). In this case, the void distribution was changed from wall peak to core or transition peak (see Fig. 2). The similar conclusion was obtained by Zun [31].

For $j_f = 1.75$, 2.62 and 3.49 m/s and $\alpha \geqslant 20\%$ (▼, ◆), the core peak in the void fraction profile was observed at the first measuring station, $L/D = 12.0$ (see Fig. 2). This might be due to the Sauter mean diameter being larger than 4.0 mm at $L/D = 12.0$ (see Fig. 4). In such a flow condition, not only large liquid turbulence but also large void fraction, namely short distance between bubbles, would increase the bubble collision frequency, resulting in cap bubbles as shown in Fig. 5. The cap bubbles formed around the pipe center might not be disintegrated because most of the turbulence kinetic energy was produced and dissipated near the wall. Large shear-induced turbulence in the vicinity of the wall would contribute to bubble breakup. As a consequence, the Sauter mean diameter profiles came to have the core peak. On the other hand, the change of area averaged Sauter mean diameter would be determined by the balance of bubble coalescence and breakup as mentioned above (see fig.6).

For $j_f = 2.62$ and 3.49 m/s, and $\alpha < 20\%$ (●, ▲, ■), the intermediate peak in the void profiles was observed. The relatively large turbulence or mixing length caused wider wall peak, namely the intermediate peak. For $\alpha \leqslant 10\%$ (●, ▲), Sauter mean diameter was smaller than 3.5 mm at the locations of $L/D = 12.0$ and 125, resulting in no significant change of the void fraction profile along the flow direction. On the other hand, for $\alpha > 10\%$ (■), Sauter mean diameter was larger than 3.5 mm at the location of $L/D = 125$, resulting in the change of the void fraction profile from the intermediate peak to the core peak along the flow direction.

3.1.2. Sauter mean diameter

For $j_f \geqslant 1.75$ m/s and $\alpha \geqslant 20\%$ (▼, ◆), the core peak in the Sauter mean diameter profile was observed (see Fig. 4). The reason would be due to the migration of large bubbles including cap bubbles toward the tube center. In other flow conditions, Sauter mean diameters were smaller than 3.5 mm and were almost uniform along the radius of the test section with some decrease in size near the wall. The wall peak in the Sauter mean diameter profile seemed to be accompanied with that in void fraction profile (see Fig. 2). The profiles were not changed significantly as the flow developed, although the bubble size increased up to 20–30% along the flow direction due to the bubble coalescence and expansion (see Fig. 6). As mentioned in Section 2.1, the reason for the decrease of Sauter mean diameter near the wall may be explained from the fact that the presence of the wall does not allow the arc length at which the bubble is intercepted by the sensor to be a random variable as in the other positions in the pipe [22].

3.1.3. Interfacial area concentration

Fig. 7 shows the behavior of interfacial area concentration profiles, corresponding to that of void fraction profiles in Fig. 2. As expected for bubbly flow, the interfacial area concentration profiles were similar to the void fraction profiles except those at $L/D = 125$ for $j_f \geqslant 1.75$ m/s and $\alpha \geqslant 20\%$ (▼, ◆). Since the interfacial area concentration is directly proportional to the void fraction and the Sauter mean diameter was almost uniform in the flow channel, the interfacial area profiles displayed the same behavior as their respective void fraction profiles. As discussed above, cap bubbles were formed for $j_f \geqslant 1.75$ m/s and $\alpha \geqslant 20\%$ (▼, ◆) as shown in Fig. 5, resulting in a concave profile of the interfacial area concentration near the tube center at $L/D = 125$.

3.1.4. Turbulence intensity

Figs. 8 and 9 show the behavior of interfacial and liquid velocities, and turbulence intensity at $L/D = 12.0$ and 125 for $j_f = 0.262$ and 1.75 m/s, respectively. The symbol of open diamond means the value measured in a water single-phase flow. Generally, introduction of bubbles into the liquid flow would cause more agitated flow than in single-phase flow turbulence as shown in Fig. 8. As Serizawa and Kataoka pointed out, under certain flow conditions, the two-phase flow turbulence is reduced locally by bubbles, when compared with single-phase flow turbulence intensity for the same liquid flow rate [32]. They explained the enhancement and reduction of two-phase flow turbulence due to the

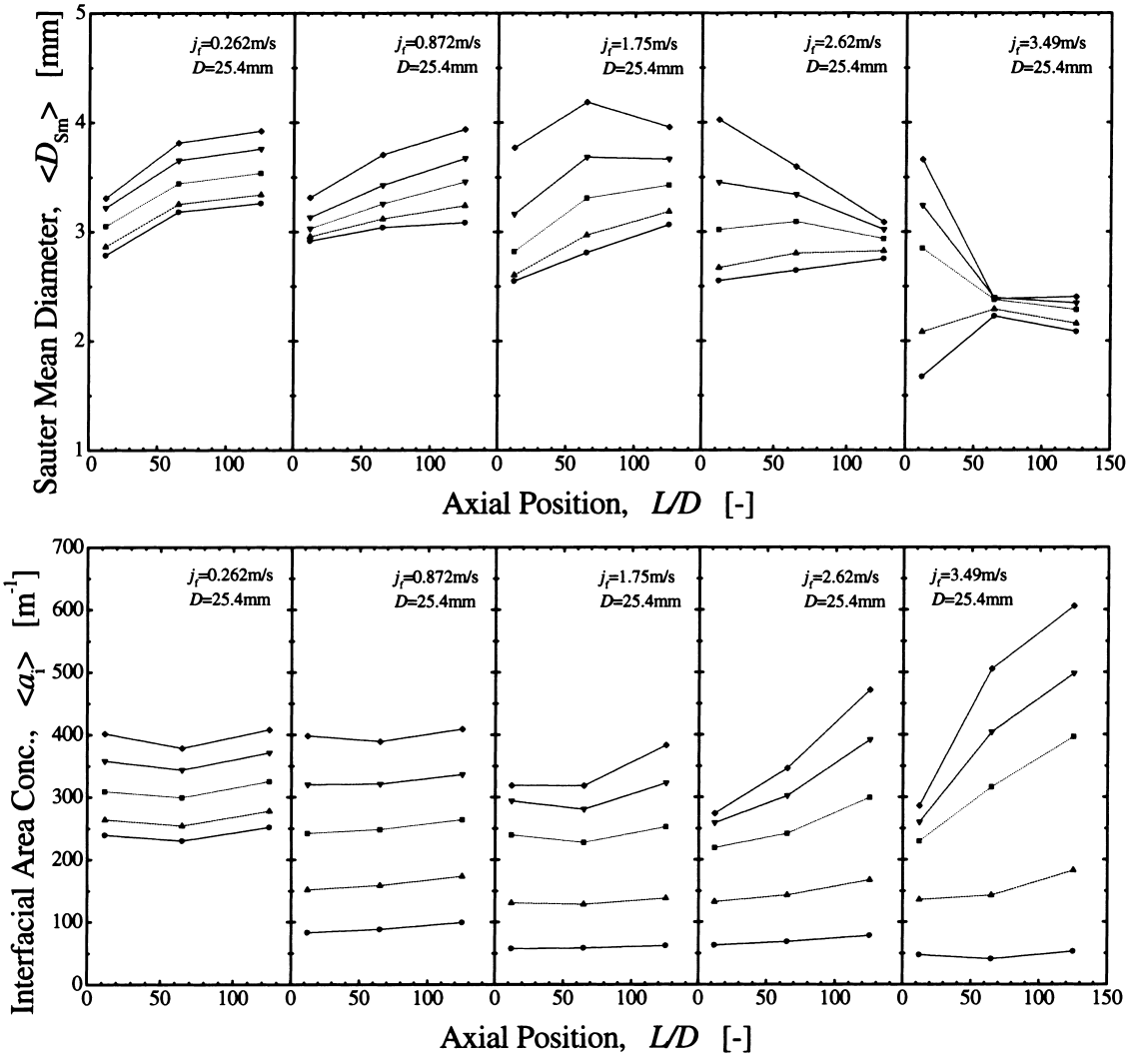

Fig. 6. Axial development of area averaged Sauter mean diameter and interfacial area concentration.

bubble introduction as follows: (1) Enhanced energy dissipation and turbulence production in the wall region due to the large gradient of the velocity fluctuation and shear stress distribution there; (2) Bubble relative motions which generate additional turbulence; (3) Large velocity fluctuation gradient near gas–liquid interfaces increases turbulence energy dissipation; and (4) Energy dumping effects of bubbles at interfaces. Serizawa and Kataoka suggested that the turbulence reduction occurred roughly at liquid velocities higher than approximately 1 m/s [32].

As can be seen in Fig. 9, slight turbulence reduction was observed for $j_f = 0.872$, 1.75, 2.62 and 3.49 m/s, and $\alpha \leqslant 5\%$, whereas the turbulence intensity enhancement phenomena was observed for $\alpha > 5\%$ regardless of the liquid velocity. For $j_f \geqslant 0.872$ m/s, the turbulence intensity for developed flows was increased from 0.03 to 0.15 as the void fraction was increased from 0 to 25%, whereas for $j_f = 0.292$ m/s, the bubble introduction ($\alpha = 0$–25%) increased the turbulence intensity significantly ($v_f'/v_{f,max} = 0.03$–0.3). For the flow conditions where the wall, transition, or intermediate peak in the void fraction profile appeared, the turbulence intensity were almost uniform with some increase near the wall (see ●, ▲, ■ in Fig. 9). Michiyoshi and Serizawa explained that this peaking in the wall region which was estimated as $D_B/R < r/R < 1$ would reflect agitating bubble motions due to bubble–wall interactions and also the interactions between bubbles and large scale liquid eddies [33]. On the other hand, for the flow conditions where the core peak appeared, the turbulence intensity had the core peak (see ▼, ◆ in Fig. 7).

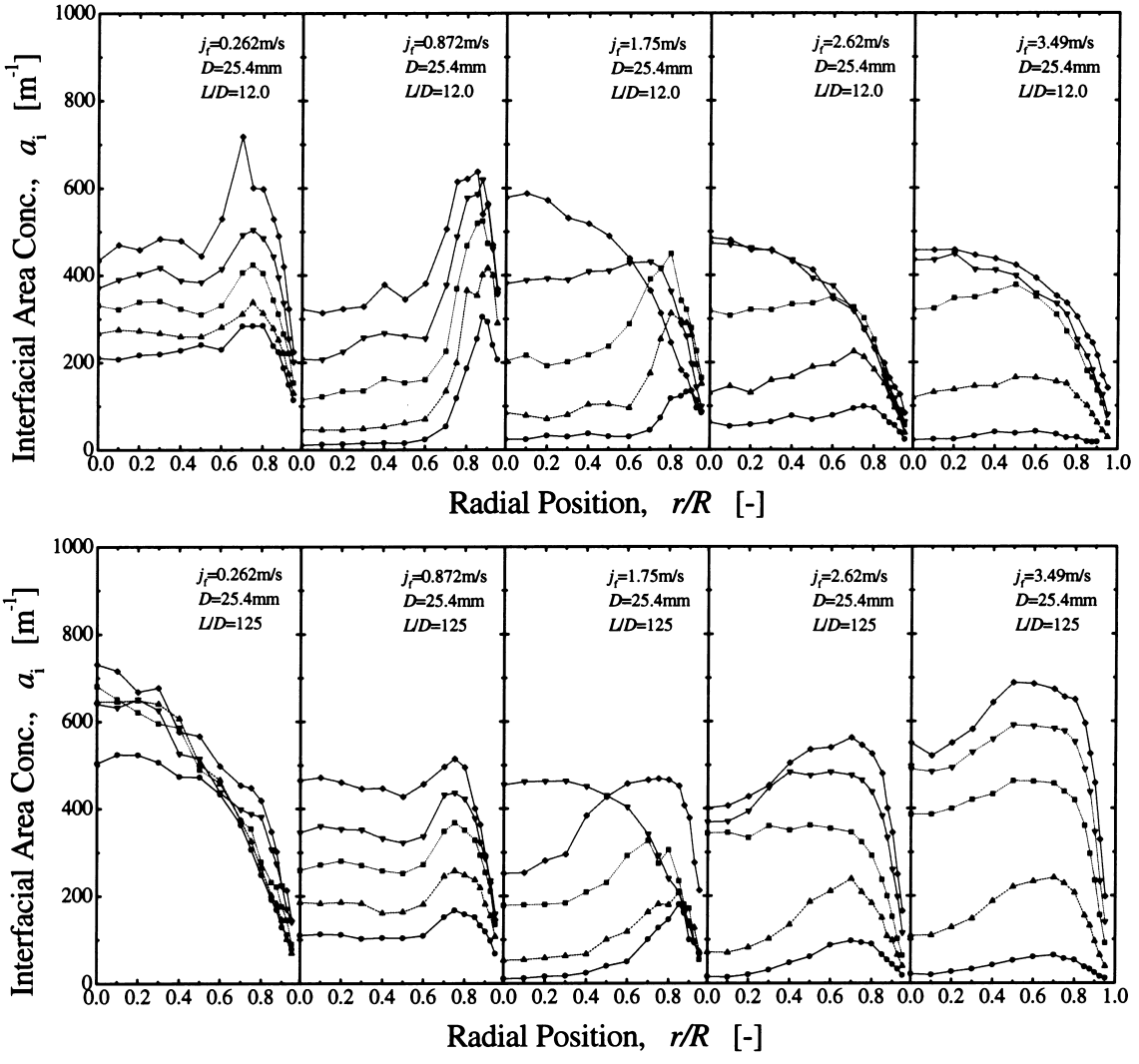

Fig. 7. Local interfacial area concentration profiles at $L/D = 12.0$ and 125.

This may be due to bubble-induced turbulence around the tube center. The turbulence intensity profiles for $j_f = 0.292$ m/s were changed from flat with some increase near the wall ($L/D = 12.0$) to core peak ($L/D = 125$), as the void fraction profiles were changed from the wall peak to the core peak.

3.1.5. Interfacial and liquid velocities

In the previous experiments using 50.8 mm-diameter pipes [14,15], the following results were obtained: (a) for $j_f < 1.0$ m/s, the introduction of bubbles into the liquid flow flattened the liquid velocity profile with a relatively steep decrease close to the wall; (b) the liquid velocity profile approached to that of developed single-phase with the increase of void fraction; and (c) the effect of the bubble on the liquid velocity profile was diminishing with increasing gas and liquid velocities. The liquid velocity profiles at $L/D = 12.0$ were flatter along the tube radius with steep decrease near the wall. However, for developed flows ($L/D = 125$) in the present experiment using the 25.4 mm pipe, the effect of the bubble injection on the liquid velocity profile were not marked even for $j_f < 1.0$ m/s as shown in Fig. 8. The liquid velocity profiles for developed flows were approximately similar to those for developed single-phase flow. The interfacial velocity profiles had the same tendency of the respective liquid velocity profiles.

3.2. One-dimensional interfacial area transport

In order to develop the one-dimensional interfacial area transport equation, an accurate data set of the

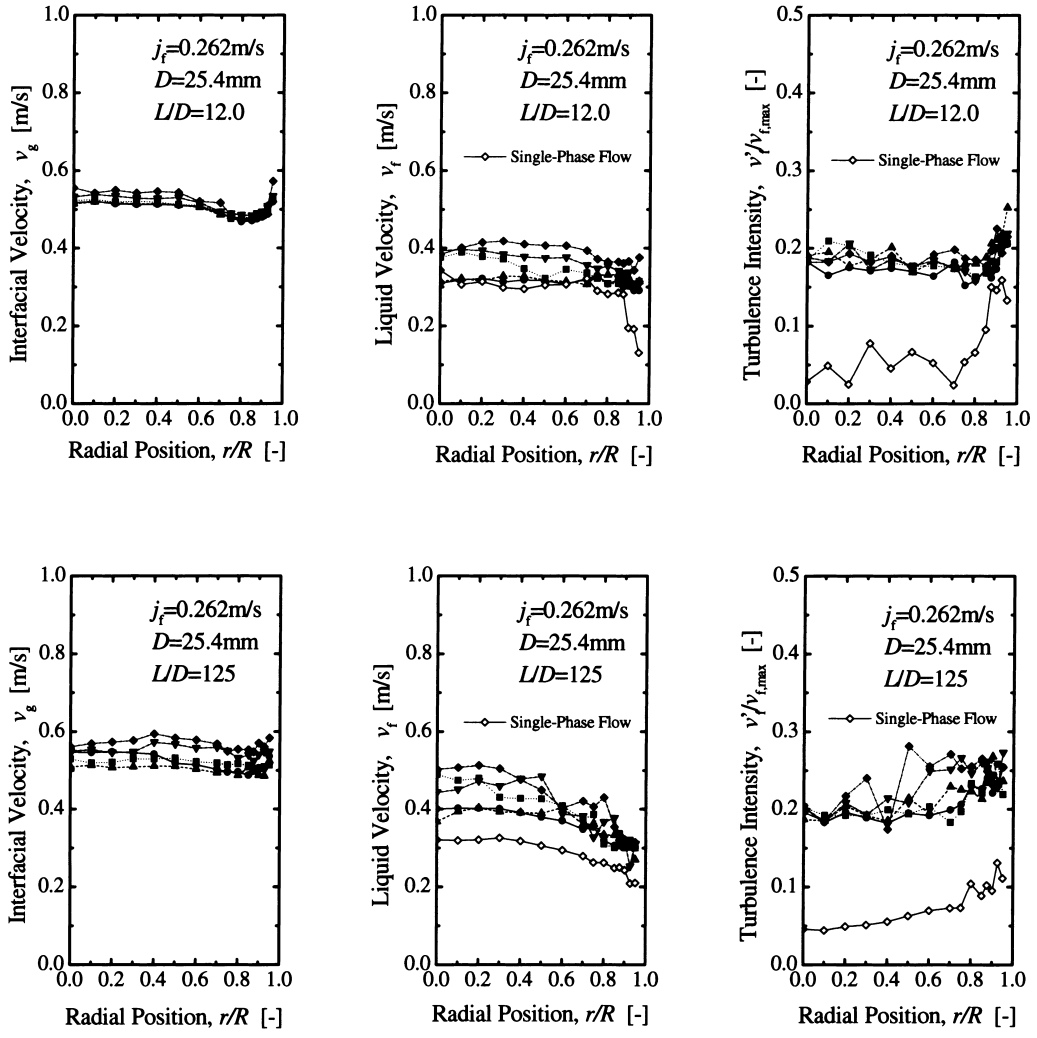

Fig. 8. Local interfacial velocity, liquid velocity, and turbulence intensity for $j_f = 0.262$ m/s at $L/D = 12.0$ and 125.

area averaged flow parameters is indispensable. One-dimensional Sauter mean diameter and interfacial area concentration are plotted against L/D in Fig. 6. For low liquid velocities such as $j_f = 0.262$, 0.871, and 1.75 m/s, the Sauter mean diameter or the interfacial area concentration increased along the axial direction gradually or concavely, respectively. On the other hand, for high liquid velocities such as $j_f = 2.62$ and 3.49 m/s and high void fraction, the Sauter mean diameter or the interfacial area concentration decreased or increased along the axial direction, respectively. The bubble expansion due to the pressure decrease and the bubble breakup, and the bubble coalescence can be thought of as the source and sink terms of the interfacial area concentration, respectively. The effect of the bubble coalescence and breakup on the interfacial area transport can be extracted as follows.

Ishii et al. derived the following interfacial area transport equation taking the gas expansion along the flow direction into account [3].

$$\frac{\partial a_i}{\partial t} + \nabla(a_i \vec{v}_g) = \frac{1}{3\psi}\left(\frac{\alpha}{a_i}\right)^2 \left[\sum_j S_j + S_{ph}\right] + \left(\frac{2a_i}{3\alpha}\right)\left[\frac{\partial \alpha}{\partial t} + \nabla(\vec{v}_g \alpha)\right] \quad (3)$$

where ψ and $\vec{v}_g$ are the factor depending on the shape of a bubble ($1/36\pi$ for a spherical bubble) and the average local bubble velocity weighted by the bubble number, respectively, and S_j, and S_{ph} denote the source or sink terms in the interfacial area concentration due to the bubble coalescence or breakup, and the phase change, respectively. Eq. (3) can be

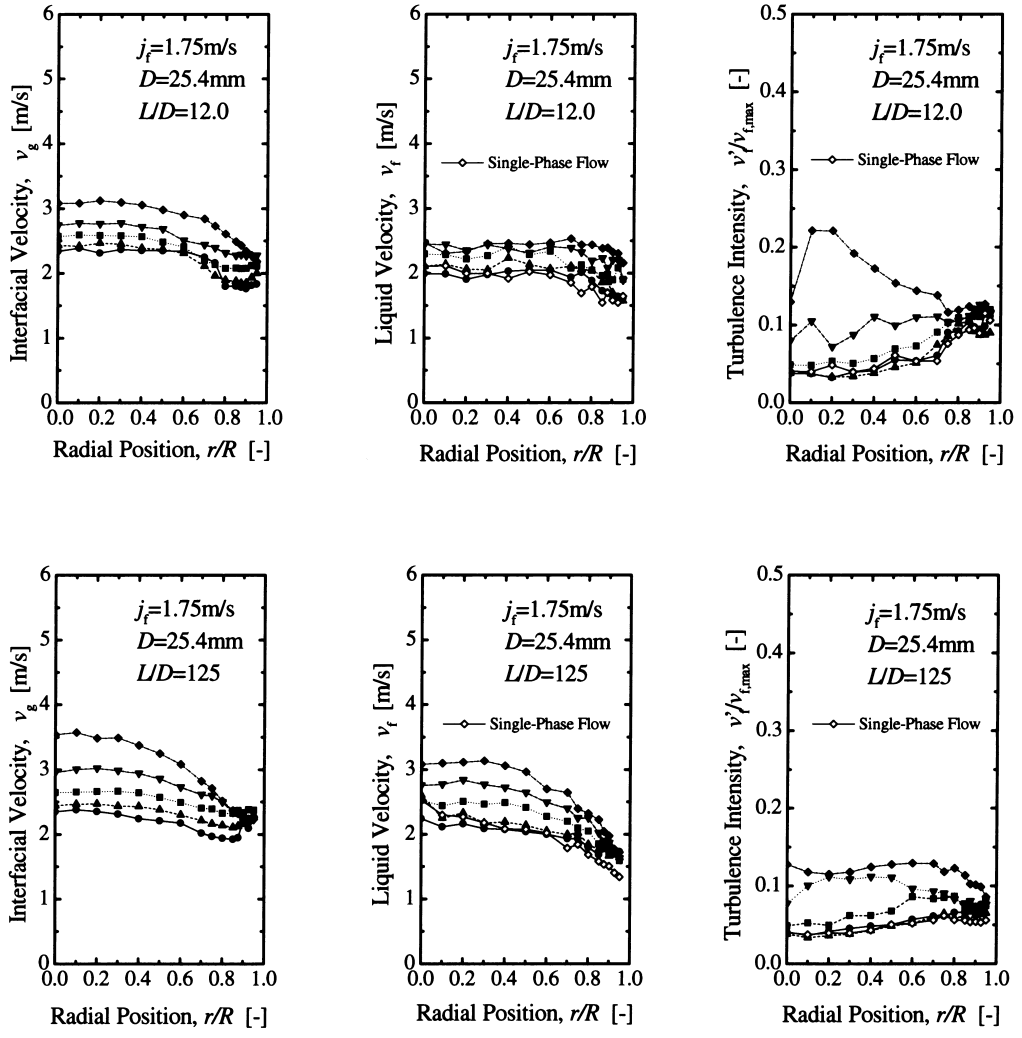

Fig. 9. Local interfacial velocity, liquid velocity, and turbulence intensity for $j_f = 1.75$ m/s at $L/D = 12.0$ and 125.

simplified as follows on the assumption of no phase change, steady flow, equilibrium of bubble coalescence and breakup rates, and one-dimensional flow.

$$a_{i,eq} = \left(\frac{P_0}{P}\right)^{2/3} a_{i,0} \tag{4}$$

where $a_{i,eq}$, $a_{i,0}$, P, and P_0 denote the local interfacial area concentration under the conditions of no phase change and equilibrium of bubble coalescence and breakup rates, the inlet interfacial area concentration, the local pressure, and the inlet pressure, respectively. The ratio of local interfacial area concentration a_i to $a_{i,eq}$, ξ ($\equiv a_i/a_{i,eq}$) represents the change in the interfacial area concentration due to the bubble coalescence and breakup. $\xi > 1$ or $\xi < 1$ implies that the bubble breakup or coalescence is dominant, respectively. It should be noted here that ξ becomes identical to a bubble number density ratio if further assumptions such as a spherical bubble and a uniform bubble distribution are made.

$$\frac{a_i}{a_{i,0}} = \frac{a_i}{a_{i,eq}}\left(\frac{P_0}{P}\right)^{2/3} = \xi\left(\frac{P_0}{P}\right)^{2/3}, \quad \xi \equiv \frac{a_i}{a_{i,eq}} \tag{5}$$

The changes in the interfacial area concentration due to the bubble coalescence and breakup ξ are plotted against L/D in Fig. 10. It should be noted in Fig. 10 that the interfacial area concentration at $L/D = 12.0$ was taken as $a_{i,0}$, and measured P_0 and P were used in the calculation of ξ. It can be clearly seen that for relatively low ($j_f = 0.262$, 0.872, and 1.75 m/s) and high liquid velocities ($j_f = 2.62$, and 3.49 m/s), the bubble coalescence and breakup were dominant for the

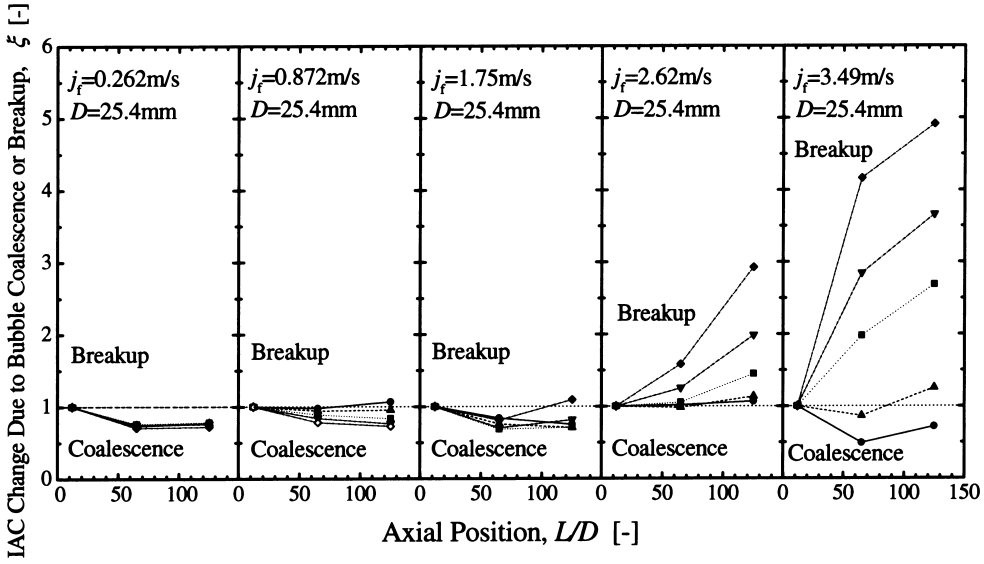

Fig. 10. Interfacial area transport due to bubble coalescence and breakup along flow direction.

interfacial area concentration change, respectively. The changes in the interfacial area concentration ξ are also plotted against a volumetric flow rate quality β ($=j_g/(j_g+j_f)$) ($\propto\alpha$) in Fig. 11. The left, middle, and right figures in Fig. 11 show the change in the interfacial area concentration between $L/D=12.0$ and 65.0, $L/D=65.0$ and 125, and $L/D=12.0$ and 125, respectively. In ξ calculations in left, middle and right figures, the interfacial area concentrations at $L/D=12.0$, 65.0, and 12.0 were taken as $a_{i,0}$. As can be seen in Fig. 11, the interfacial area concentration change was almost completed by the second measuring station, $L/D=65.0$. After $L/D=65.0$, the bubble coalescence and breakup seems to reach the steady state, particularly for low liquid velocities.

The interfacial area transport mechanism in a bubbly flow system can be roughly classified into three basic mechanisms, namely bubble coalescence due to the collision between bubbles and the bubble expansion for the sink terms, and the bubble breakup due to the collision between a bubble and a turbulence eddy for the source term. The bubble coalescence would be

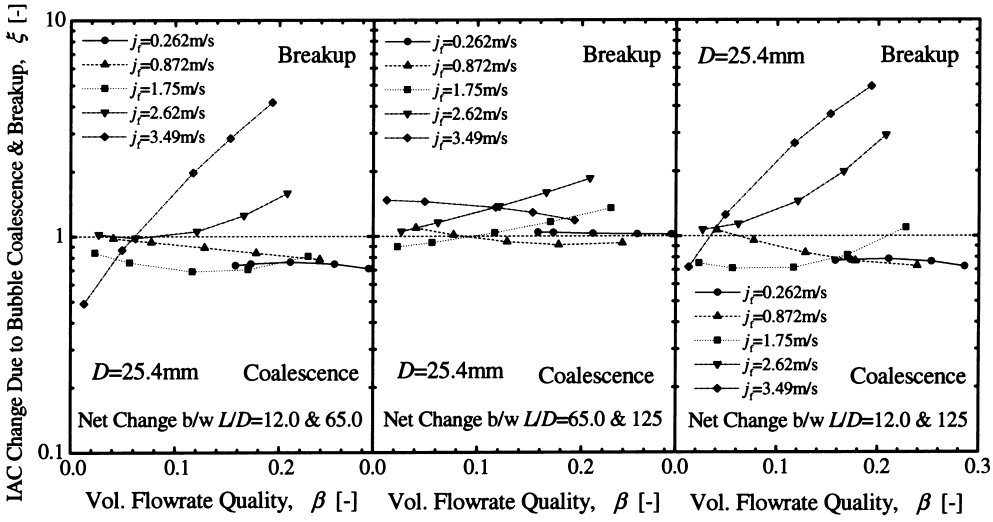

Fig. 11. Dependence of interfacial area transport due to bubble coalescence and breakup on volumetric flow quality.

governed by the collision frequency between bubbles, and the bubble coalescence efficiency. The collision frequency between bubbles would be modeled by taking account of the bubble velocity induced by the liquid turbulence, the void fraction, the bubble diameter, and so on, whereas the bubble coalescence efficiency might be modeled by taking account of the bubble contact time for two bubbles and the time required for coalescence of bubbles. On the other hand, the bubble breakup would be governed by the collision frequency between bubbles and eddies, and the bubble breakup efficiency. The collision frequency between bubbles and eddies would be modeled by taking account of the relative velocity between bubbles and eddies, the void fraction, the eddy fraction, the bubble diameter, and so on, whereas the bubble breakup efficiency might be modeled by the eddy energy and the energy required for bubble breakup.

For low liquid velocity and void fraction, the weak interactions of bubble–bubble and bubble–eddy due to small liquid turbulence and bubble mixing length would cause $\xi \approx 1$ (see Fig. 11). Although the increase in void fraction would promote the frequency of the collision between bubbles as well as that of between bubbles and eddies, the liquid turbulence might not be large enough to breakup the bubble. Consequently, the bubble coalescence rates were increased gradually with the void fraction increases. On the other hand, for high liquid velocities, the bubble breakup rates were increased with the void fraction, since the increase in void fraction would decrease not only the distance between the bubble and the turbulent eddy, namely the collision frequency between bubbles and eddies, but also the liquid velocity, namely the liquid turbulence.

4. Conclusions

In relation to the development of the interfacial area transport equation, local measurements of the void fraction, interfacial area concentration, interfacial velocity, and Sauter mean diameter using the double sensor probe method as well as the liquid velocity and turbulence intensity using hotfilm anemometry were performed extensively for vertical upward bubbly air–water flows in a round tube with an inner diameter of 25.4 mm at three axial locations of $L/D = 12.0$, 65.0 and 125, and fifteen radial locations from $r/R = 0$ to 0.95. The liquid flow rate and the void fraction ranged from 0.292 m/s to 3.49 m/s and from 3% to 27%, respectively.

The mechanisms on the radial profiles of local flow parameters and their axial developments were discussed. In order to understand the mechanism of one-dimensional interfacial area transport, the change of the interfacial area concentration due to the bubble coalescence and breakup was displayed as a function of the volumetric flow quality. For low liquid velocities, the bubble coalescence rates were increased gradually with the void fraction increases. In the flow region, although the increase in void fraction would promote the bubble–bubble interaction, the liquid turbulence might not be large enough to break up the bubble. On the other hand, for high liquid velocities, the bubble breakup rates were increased with the void fraction, since the increase in void fraction decreased not only the distance between the bubble and the turbulent eddy but also the liquid velocity, namely the liquid turbulence. Thus, it turned out that the mechanism of the interfacial area transport depended on the bubble mixing length, turbulence intensity, void fraction, and so on.

The combined data from the double sensor probe and the hot film probe gave the near complete information on the time averaged local hydrodynamic parameters of two-phase flow. The data set obtained in this study will eventually be used for the development of reliable constitutive relations which reflect the true transfer mechanisms in bubbly flow systems.

Acknowledgements

The authors would like to acknowledge Dr Leung (Royal Institute of Technology, Sweden), Prof Wu (Oregon State University, USA) and Prof Bertodano (Purdue University, USA) for their valuable discussions. The authors wish to thank Mr F. Takada (Kyushu Electric Company, Japan) for his assistance in the experiment. This work was performed under the auspices of the US Department of Energy's Office of Basic Energy Science. The authors would like to express their sincere appreciation for the encouragement, support and technical comments on this program from Drs Manley, Goulard, and Price of DOE/BES.

Appendix A

To model the source and sink terms in the interfacial area transport equation caused by bubble coalescence and breakage, a general approach treats the bubbles in two groups: the spherical/distorted bubble group and the cap/slug bubble group, resulting in two interfacial area transport equations that involve the inner and inter group interactions [5]. In practice, when the void fraction of a two-phase bubbly flow is small, no cap or slug bubbles exist. The two-group transport equations are then reduced to one-group without the involvement of the interactions between the two groups. The purpose of this study is to provide a rigorous data base to

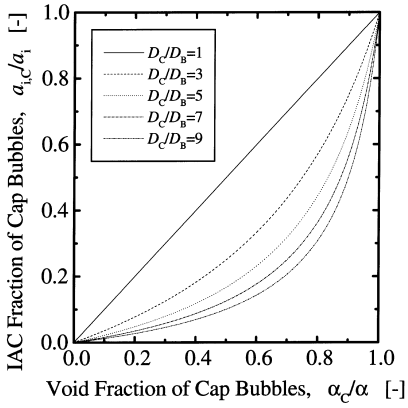

Fig. A1. Contribution of cap bubbles to total interfacial area concentration.

develop the source and sink terms in one-group transport equation as a first step. An advanced measuring technique such as the multi-sensor probe method [34] should be used for a future study on the interfacial area concentration measurement of cap and slug bubbles. Therefore, the data taken at the bubbly flow regime can be primarily utilized to verify modeled sink and source terms in one-group interfacial area transport equation. In addition to this, when the fraction of cap bubbles is relatively small, obtained data can probably be used for the verification on the following grounds.

Assuming the uniform size distribution of small and cap bubbles, the void fractions for small and cap bubbles are given by:

$$\alpha_B = \frac{\pi}{6} D_B^3 n_B, \quad \alpha_C = \frac{\pi}{6} D_C^3 n_C \tag{A1}$$

where D_B and D_C mean the sphere equivalent diameters of small and cap bubbles, respectively. n_B and n_C denote the bubble number densities of small and cap bubbles, respectively. The number of density ratio of cap bubbles to all bubbles can be deduced as:

$$\frac{n_C}{n_B} = \frac{\alpha_C}{\alpha - \alpha_C} \frac{D_B^3}{D_C^3} \tag{A2}$$

The contribution of cap bubbles to the total interfacial area concentration is expressed by:

$$\frac{a_{i,C}}{a_i} = \frac{\eta_C n_C D_C^2}{\eta_B n_B D_B^2 + \eta_C n_C D_C^2} \tag{A3}$$

where η_B and η_C denote the correction factors due to the bubble deformation for small and cap bubbles, respectively, of the order 1. For example, when a spherical bubble is transformed into an ellipsoidal bubble with the aspect ratio of 2, the resulting increase of the interfacial area is estimated mathematically to be 9.5%, namely $\eta = 1.095$. Here, assuming $\eta_B = \eta_C$ for simplicity, Eq. (A3) is simplified as:

$$\frac{a_{i,C}}{a_i} = \frac{(n_C/n_B) D_C^2}{D_B^2 + (n_C/n_B) D_C^2} = \frac{(\alpha_C/\alpha)}{D_C/D_B + (1 - D_C/D_B)(\alpha_C/\alpha)} \tag{A4}$$

In Fig. A1, the interfacial area concentration fraction of cap bubbles $a_{i,C}/a_i$ is plotted against the void fraction of cap bubbles α_C/α as a parameter of the bubble diameter ratio D_C/D_B. At bubbly-to-slug flow transition, D_C/D_B would be roughly larger than 5; for example, $D_C/D_B = 5$ for $D_C = 20$ mm and $D_B = 4$ mm. The figure implies that the contribution of cap bubbles to total interfacial area concentration would be less than 10% even for $\alpha_C/\alpha \approx 0.4$. Therefore, it is expected that even data taken at the bubbly-to-slug transition would be used for evaluation of modeled sink and source terms in one-group interfacial area transport equation.

References

[1] M. Ishii, Thermo-Fluid Dynamic Theory of Two-Phase Flow, Eyrolles, Paris, 1975.
[2] G. Kocamustafaogullari, M. Ishii, Foundation of the interfacial area transport equation and its closure relations, International Journal of Heat and Mass Transfer 38 (1995) 481–493.
[3] M. Ishii, Q. Wu, S.T. Revankar, T. Hibiki, W.H. Leung, S. Hogsett, A. Kashyap, Interfacial area transport in bubbly flow, in: Proceedings of 15th Symposium on Energy Engineering Science, Argonne, USA, 1997.
[4] Q. Wu, S. Kim, M. Ishii, S.G. Beus, One-group interfacial area transport in vertical air–water bubbly flow, in: ANS Proceedings of 1997 National Heat Transfer Conference, HTC-Vol.10, ANS, Baltimore, USA, 1997, pp. 67–79.
[5] Q. Wu, S. Kim, M. Ishii, S.G. Beus, One-group interfacial area transport in vertical bubbly flow, International Journal of Heat and Mass Transfer 41 (1998) 1103–1112.
[6] A. Serizawa, I. Kataoka, I. Michiyoshi, Turbulence structure of air–water bubbly flow—I. Measuring techniques, International Journal of Multiphase Flow 2 (1975) 221–233.
[7] A. Serizawa, I. Kataoka, I. Michiyoshi, Turbulence structure of air–water bubbly flow—II. Local properties, International Journal of Multiphase Flow 2 (1975) 235–246.
[8] A. Serizawa, I. Kataoka, I. Michiyoshi, Turbulence structure of air–water bubbly flow—III. Transport properties, International Journal of Multiphase Flow 2 (1975) 247–259.
[9] S.K. Wang, S.J. Lee, O.C. Jones Jr, R.T. Lahey Jr, 3-D

turbulence structure and phase distribution measurements in bubbly two-phase flows, International Journal of Multiphase Flow 13 (1987) 327–343.

[10] M.L. Bertodano, Turbulent bubbly two-phase flow in a triangular duct. PhD. Thesis, Rensselaer Polytechnic Institute, New York, USA, 1992.

[11] T.J. Liu, S.G. Bankoff, Structure of air–water bubbly flow in a vertical pipe—I. Liquid mean velocity and turbulence measurements, International Journal of Heat and Mass Transfer 36 (1993) 1049–1060.

[12] T.J. Liu, S.G. Bankoff, Structure of air-water bubbly flow in a vertical pipe—II. Void fraction, bubble velocity and bubble size distribution, International Journal of Heat and Mass Transfer 36 (1993) 1061–1072.

[13] C. Grossetete, Experimental investigation and preliminary numerical simulations of void profile development in a vertical cylindrical pipe, in: Proceedings of Second International Conference on Multiphase Flow '95, Kyoto, Japan, vol. 2, 1995, pp. IF1-1–IF1-10.

[14] T. Hibiki, S. Hogsett, M. Ishii, Local measurement of interfacial area, interfacial velocity and liquid turbulence in two-phase flow, in: Proceedings of OECD/CSNI Specialist Meeting on Advanced Instrumentation and Measurement Techniques, Santa Barbara, USA, Session IV, 1997 to be published in Nuclear Engineering and Design.

[15] T. Hibiki, M. Ishii, Z. Xiao, Local flow measurements of vertical upward air–water flow in a round tube, in: Proceedings of Third International Conference on Multiphase Flow '98, Lyon, France, 1998.

[16] T. Hibiki, S. Hogsett, M. Ishii, Axial development of liquid turbulence and interfacial area in bubbly two-phase flows, PU/NE-97-2, Purdue University, IN, USA, 1997.

[17] I. Kataoka, M. Ishii, A. Serizawa, Local formulation and measurements of interfacial area concentration in two-phase flow, International Journal of Multiphase Flow 12 (1984) 505–529.

[18] Q. Wu, D. Zheng, M. Ishii, S.G. Beus, Measurements of interfacial area concentration in two-phase flow with two-point conductivity probe. International Journal of Multiphase Flow (submitted).

[19] T. Hibiki, W.H. Leung, M. Ishii, Measurement method of local interfacial area in two-phase flow using a double sensor probe, PU/NE-97-5, Purdue University, IN, USA, 1997.

[20] W. Hilgert, H. Hofmann, Characterization of gas phase flow in bubble columns at low superficial gas velocities with the aid of ultrasonic Doppler techniques, Germany Chemical Engineering 9 (1986) 180–190.

[21] S.T. Revankar, M. Ishii, Local interfacial area measurement in bubbly flow, International Journal of Heat and Mass Transfer 35 (1992) 913–925.

[22] S. Kalkach-Navarro, R.T. Lahey Jr, D.A. Drew, R. Meyder, Interfacial area density, mean radius and number density measurements in bubbly two-phase flow, Nuclear Engineering and Design 142 (1993) 341–351.

[23] W.H. Leung, S.T. Revankar, Y. Ishii, M. Ishii, Axial development of interfacial area and void concentration profiles measured by double-sensor probe method, International Journal of Heat and Mass Transfer 38 (1995) 445–453.

[24] W.H. Leung, C.S. Eberle, Q. Wu, T. Ueno, M. Ishii, Quantitative characterizations of phasic structure developments by local measurement methods in two-phase flow, in: Proceedings of Second International Conference on Multiphase Flow '95, Kyoto, Japan, 1, IN2-17, 1995.

[25] R. Clift, J.R. Grace, M.E. Weber, Bubbles, Drops, and Particles, Academic Press, New York, USA, 1978.

[26] T. Hibiki, W.H. Leung, M. Ishii Measurement method of local turbulence in two-phase flow using hotfilm anemometry, PU/NE-97-6, Purdue University, IN, USA, 1997.

[27] I. Kataoka, A. Serizawa, Interfacial area concentration in bubbly flow, Nuclear Engineering and Design 120 (1990) 163–180.

[28] T.J. Liu, Bubble size and entrance length effects on void development in a vertical channel, International Journal of Multiphase Flow 19 (1993) 99–113.

[29] A. Serizawa, I. Kataoka, Phase distribution in two-phase flow, in: N.H. Afgan (Ed.), Transient Phenomena in Multiphase Flow, Hemisphere, Washington, DC, USA, 1988, pp. 179–224.

[30] Y. Taitel, D. Bornea, E.A. Dukler, Modelling flow pattern transitions for steady upward gas-liquid flow in vertical tubes, AIChE Journal 26 (1980) 345–354.

[31] I. Zun, Transition from wall void peaking to core void peaking in turbulent bubbly flow, in: N.H. Afgan (Ed.), Transient Phenomena in Multiphase Flow, Hemisphere, Washington, DC, USA, 1988, pp. 225–245.

[32] A. Serizawa, I. Kataoka, Turbulence suppression in bubbly two-phase flow, Nuclear Engineering and Design 122 (1990) 1–16.

[33] I. Michiyoshi, A. Serizawa, Turbulence in two-phase bubbly flow, Nuclear Engineering and Design 95 (1986) 253–267.

[34] S.T. Revankar, M. Ishii, Theory and measurement of local interfacial area using a four sensor probe in two-phase flow, International Journal of Heat and Mass Transfer 36 (1993) 2997–3007.